Agència de Gestió d'Ajuts Universitaris i de Recerca

Memòria justificativa de recerca de les convocatòries BE, PIV, BCC, NANOS i BP

La memòria justificativa consta de les dues parts que venen a continuació:
1.- Dades bàsiques i resums
2.- Memòria del treball (informe científic)

Tots els camps són obligatoris

1.- Dades bàsiques i resums

Nom de la convocatòria

PIV

Llegenda per a les convocatòries:

BCC	Convocatòria de beques per a joves membres de comunitats catalanes a l'exterior (BCC)
BE	Beques per a estades per a la recerca fora de Catalunya (BE)
BP	Convocatòria d'ajuts postdoctorals dins del programa Beatriu de Pinós (BP)
NANOS	Beques de recerca per a la formació en el camp de les nanotecnologies (NANOS)
PIV	Beques de recerca per a professors i investigadors visitants a Catalunya (PIV)

Títol del projecte: ha de sintetitzar la temàtica científica del vostre document.
Innovació Tecnològica a la Construcció Subterrània

Dades de l'investigador

Nom	Cognoms
Jerzy	**Rojek**

Correu electrònic
rojek@cimne.upc.edu

Dades del centre d'origen
Institute of Fundamental Technological Research of Polish Academy of Sciences in Warsaw

Número d'expedient
2006PIV 00018

Paraules clau: cal que esmenteu cinc conceptes que defineixin el contingut de la vostra memòria.
enginyeria geològica, excavacions subterrànies, mètodes numèrics, mètodes de partícules, simulació numèrica.

Data de presentació de la justificació
19/12/2008

Resum del projecte: cal adjuntar dos resums del document, l'un en anglès i l'altre en la llengua del document, on s'esmenti la durada de l'acció

Resum en la llengua del projecte (màxim 300 paraules)

En Jerzy Rojek es va unir a un grup de recerca de CIMNE que desenvolupa mètodes numèrcs per a l'anàlisi de problemes d'enginyeria complexos, que van des de l'enginyeria civil fins a les tecnologies de fabricació. Ha contribuït amb la seva experiència en el camp dels mètodes d'elements finits i dels mètodes d'elements discrets, utilitzant algoritmes basats en la integració en temps explícit, molt eficient per a la solució de problemes d'enginyeria de grans dimensions.

En particular, en Rojek ha treballat en el projecte europeu TUNCONSTRUCT (Technology innovation in underground construction, VI FP, Ref: NMP2-CT-2005-011817, 01/09/2005 - 30/08/2009). El Dr. Rojek ha liderat el grup de recerca de CIMNE que ha treballat en aquest projecte. CIMNE té un paper molt important a TUNCONSTRUCT, especialment en les tasques de desenvolupament de software per a l'anàlisi d'excavacions subterrànies. En particular, aquestes són les tasques que ha realitzat el Dr. Rojek durant l'estada de 2007:

• desenvolupament del software per a la modelització d'excavacions subterrànies basat en el mètode dels elements discrets. Els algortitmes numèrics s'han implementat en programes d'ordinador i s'han aplicat per a la simulació d'excavacions
• acoblament del mètode dels elements discrets amb el mètode dels elements finits – utilitzar els dos mètodes i tractar-los com a complementaris va permetre incrementar l'eficiència de l'anàlisi numèrica d'estructures subterrànies
• desenvolupament del model numèric de tall de roca tenint en compte el desgast de les eines de tall

Les tasques desenvolupades s'han recollit en informes tècnics i en articles científics, incloent 5 papers que s'han presentat a la Conferència ECCOMAS (EURO-TUN 2008) i a la Conferència Computational Plasticity (COMPLAS 2007). Un article ha estat acceptat en una revista del SCI, i els altres dos articles s'han presentat per a publicació en revistes del SCI.

Durant la seva estada a CIMNE, el Dr. Rojek ha impartit 5 seminaris en els quals ha presentat la formulació teòrica i la implementació del mètode dels elements discrets.
El Dr. Rojek ha treballat en la preparació de nous projectes europeus, un d'ells conjuntament amb la Technical University of Graz.

Resum en anglès(màxim 300 paraules)

Jerzy Rojek joined a research group of CIMNE developing numerical methods for analysis for complex engineering problems ranging from civil engineering to manufacturing technology. He has contributed with his experience in the field of the finite element method and discrete element method, employing the algorithms based on the explicit time integration, very efficient in the solution of large engineering problems.

In particular he dedicated himself to work in the European project TUNCONSTRUCT (Technology innovation in underground construction, the Sixth Framework Programme, Ref: NMP2-CT-2005-011817, 01/09/2005 - 30/08/2009. He leadered the research group of CIMNE working in this project. CIMNE has a very important role to play in the TUCONSTRUCT project in the tasks dedicated to the development of the software for analysis of underground excavation, In particular the following tasks were realized by Jerzy Rojek and the CIMNE research group headed by him in 2007:

• Development of the software for modeling underground excavation based on the discrete element method. The numerical algorithms have been implemented in the computer programs and applied to simulation of excavation using roadheaders and TBM-s.

• Coupling of the discrete element method with the finite element method – employing the two different methods and treating them as complimentary allowed us to increase efficiency of numerical analysis of underground structures.

• Development of the numerical model of rock cutting taking into account of wear of rock cutting tools. This work considers a very important factor influencing effectiveness of underground works.

The work has been described in the technical reports as well as scientific articles, including 5 papers presented in the ECCOMAS conference EURO:TUN 2008, one paper presented in the Complas conference in 2007. One paper has been accepted for publication in a SCI journal, two more papers have been submitted for publication in SCI journals.

During his stay in CIMNE J. Rojek has given 5 seminars presenting theoretical formulation and implementation of the discrete element method.

J. Rojek worked on preparation of new EC projects, one project was prepared together with the Technical University of Graz.

2.- Memòria del treball (informe científic sense limitació de paraules). Pot incloure altres fitxers de qualsevol mena, no més grans de 10 MB cadascun d'ells.

La memòria del treball es presenta en un document a part (Memòria del Treball - Jerzy Rojek.pdf).

Agència de Gestió d'Ajuts Universitaris i de Recerca

L'AGAUR inclourà a RECERCAT la memòria justificativa en versió digital. Per aquest motiu, us demanem el vostre consentiment per introduir a RECERCAT el contingut científic de la vostra justificació de recerca. Si esteu d'acord amb aquesta proposta, cal que llegiu la **llicència Creative Commons** i ens envieu el document que us adjuntem imprès, omplert i signat a:

Programa de documentació científica
Agència de Gestió d'Ajuts Universitaris i de Recerca
Via Laietana, 28 2na planta
08003 Barcelona

RECERCAT

La persona sotasignant, , en qualitat de beneficiària de l'ajut de l'Agència de Gestió d'Ajuts Universitaris i de Recerca (AGAUR), amb núm d'expedient, manifesta el seu consentiment exprés per tal que la justificació presentada en el marc de l'esmentat ajut sigui introduïda al dipòsit digital RECERCAT del Consorci de Biblioteques Universitàries de Catalunya, d'acord amb els termes especificats a la llicència Creative Commons de Reconeixement-No-Comercial-SenseObra Derivada.

Aquesta llicència estableix que es permet copiar, distribuir i comunicar públicament l'obra sempre que se'n citi l'autor original i la institució que l'empara i no se'n faci cap ús amb finalitats comercials ni obra derivada. Per obra derivada s'entén aquell document que ha estat editat, traduït, combinat amb materials de tercers, canviat de format, o modificat de qualsevol altra forma.

☒ Sí, estic d'acord amb el text anterior.
☐ No, no estic d'acord.

Barcelona, 19 de desembre de 2008

Signatura
DNI

Aquelles persones o institucions que ho requereixin, amb una adequada argumentació, podran sol·licitar, si escau, un retràs màxim de dos anys per introduir la memòria justificativa a Recercat.

TECHNOLOGY INNOVATION IN UNDERGROUND CONSTRUCTION

Jerzy Rojek

International Center for Numerical Methods in Engineering
Edifici C1, Campus Nord UPC, Gran Capitán s/n, 08034 Barcelona, Spain
e-mail: rojek@cimne.upc.edu

SUMMARY

This report presents the most important results of the work carried out by the author and/or under his supervision during his stay in the International Center for Numerical Methods in Engineering (CIMNE) in Barcelona in 2007 within the project *Technology innovation in underground construction*.

The work can be grouped into the following tasks:

- Development of the software for modeling underground excavation based on the discrete element method.
- Coupling of the discrete element method with the finite element method
- Development of the numerical model of rock cutting taking into account of wear of rock cutting tools.

Numerical model employed for simulation of underground excavation is based on the discrete element method. Discrete element formulation employing spherical (in 3D) and cylindrical (in 2D) has been developed and implemented in the CIMNE in-house code Simpact. The set of parameters for discrete element model has been established by a calibration procedure based on numerical simulation of the unconfined compression and Brazilian tests, with the results of laboratory tests for specimens of the rock under consideration as reference data. Having established model parameters, numerical simulation of cutting with a roadheader pick has been carried out. The simulation provides values and variation of cutting forces. Results of the simulation have been compared with experimental results.

A coupled discrete/finite element technique has been developed to model undeground excavation. Combining different methods in one model allows us to take advantages of each method. The discrete element method (DEM) is a suitable method to take into account all kinds of discontinuities and material failure characterized with fracture, while the finite element method (FEM) is usually a method of choice in dealing with problems involving linear and nonlinear continuous material behaviour in domains of finite dimensions.

Coupling of these two method yields an efficient model for simulation of tunnel excavation on a low scale, with rock cutting mechanism being analyzed. Discrete elements are used only in a portion of the analysed domain where material fracture occurs. Outside the DEM subdomain finite elements are used which is a more efficient approach for a continuum material. Coupling between the DEM and FEM subdomains provided by additional kinematical constraints imposed by the Lagrange multiplier or penalty method. Correct performance of the

coupling method in the presence of wave propagation has been demonstrated in different numerical benchmarks. The combined DEM/FEM modelling has been applied in simulation of undeground excavation with roadheaders and TBMs allowing us to obtain important practical results.

Estimation of wear has been included into the numerical model of rock cutting based on the discrete element method. The amount of wear is calculated using the classical formula of Archard. The wear model takes into account the influence of temperature by considering the hardness of the worn material as temperature dependent. Temperature increase due to frictional heat generation is obtained in the thermomechanical simulation of cutting. Numerical analysis yields the wear profile as well as the tool shape evolution due to wear.

The numerical model developed allows us to study the wear intensity for different cutting process parameters. The methodology developed can be employed in the design of cutting heads and cutting operations in undeground excavations with roadheaders.

1 MODELLING OF UNDERGROUND EXCAVATION WITH ROADHEADERS

1.1 Introduction

Roadheaders are most widely used underground partial-face excavation machines for low to medium strength rocks, in mining engineering as well as in excavation of different underground structures. Figure 1 shows a roadheader in a real excavation process.

Figure 1: Excavation with a roadheader

Performance prediction for the cutting heads of roadheaders and the cutting unit's optimization require knowledge about the cutting action of picks [10]. Cutting force is one of the factors limiting the tool's applications and the cutting efficiency. Theoretical evaluation of the cutting force is not an easy task. Simple analytical models, like those developed by Evans [6] or by Nishimatsu [11], can provide only very approximate estimation of cutting forces. More accuracy can be expected from models based on numerical methods. Different possibilities can be chosen for numerical modelling of rock cutting process. Despite many advantages numerical methods based on the continuum models, like finite element methods, have serious problems in modelling discontinuities of the material occuring during rock cutting [8]. The present work takes advantages of the numerical model based on the discrete element method.

1.2 Discrete element method formulation

Within the DEM, it is assumed that a solid material can be represented as a collection of rigid particles/blocks interacting among themselves in the normal and tangential directions. Particles/blocks can be of arbitrary shape, here, the spherical (in 3D) and cylindrical (in 2D) particles are employed. Discrete element formulation using spherical or cylindrical particles was first proposed by Cundall and Strack [5, 4]. Similar formulation has been developed by Rojek et al. in [17] and implemented in the explicit dynamic finite element code Simpact.

The translational and rotational motion of rigid spherical or cylindrical elements (particles) is governed by the standard equations of rigid body dynamics. For the i-th element we have

$$m_i \ddot{\mathbf{u}}_i = \mathbf{F}_i \,, \tag{1}$$

$$I_i \dot{\boldsymbol{\omega}}_i = \mathbf{T}_i \,, \tag{2}$$

where $\mathbf{u}$ is the element centroid displacement in a fixed (inertial) coordinate frame $\mathbf{X}$, $\boldsymbol{\omega}$ – the angular velocity, m – the element mass, I – the moment of inertia, $\mathbf{F}$ – the resultant force, and $\mathbf{T}$ – the resultant moment about the central axes. Vectors $\mathbf{F}$ and $\mathbf{T}$ are sums of all forces and moments applied to the i-th element due to external load, contact interactions with neighbouring spheres and other obstacles, as well as forces resulting from damping in the system. The form of the rotational equation (58) is valid for spheres and cylinders (in 2D) and is simplified with respect to a general form for an arbitrary rigid body.

Equations of motion (57) and (58) are integrated in time using a central difference scheme. The time integration operator for the translational motion at the n-th time step is as follows:

$$\ddot{\mathbf{u}}_i^n = \frac{\mathbf{F}_i^n}{m_i} \,, \tag{3}$$

$$\dot{\mathbf{u}}_i^{n+1/2} = \dot{\mathbf{u}}_i^{n-1/2} + \ddot{\mathbf{u}}_i^n \Delta t \,, \tag{4}$$

$$\mathbf{u}_i^{n+1} = \mathbf{u}_i^n + \dot{\mathbf{u}}_i^{n+1/2} \Delta t \,. \tag{5}$$

The first two steps in the integration scheme for the rotational motion are identical to those given by equations (3) and (4):

$$\dot{\boldsymbol{\omega}}_i^n = \frac{\mathbf{T}_i^n}{I_i} \,, \tag{6}$$

$$\boldsymbol{\omega}_i^{n+1/2} = \boldsymbol{\omega}_i^{n-1/2} + \dot{\boldsymbol{\omega}}_i^n \Delta t \,. \tag{7}$$

The vector of incremental rotation $\Delta\boldsymbol{\theta} = \{\Delta\theta_x \, \Delta\theta_y \, \Delta\theta_z\}^{\mathrm{T}}$ is calculated as

$$\Delta\boldsymbol{\theta}_i = \boldsymbol{\omega}_i^{n+1/2} \Delta t \,, \tag{8}$$

If necessary it is also possible to track the total change of rotational position of particles.

Explicit integration in time yields high computational efficiency of the solution for a single step. The disadvantage of the explicit integration scheme is its conditional numerical stability imposing the limitation on the time step Δt. The time step Δt must not be larger than a critical time step Δt_{cr}

$$\Delta t \leq \Delta t_{\mathrm{cr}} \tag{9}$$

determined by the highest natural frequency of the system $\omega_{\max}$

$$\Delta t_{\mathrm{cr}} = \frac{2}{\omega_{\max}} \,. \tag{10}$$

Exact determination of the highest frequency $\omega_{\max}$ would require solution of the eigenvalue problem defined for the whole system of connected rigid particles. In an approximate solution procedure adopted, the maximum frequency is estimated as the maximum of natural frequencies of mass–spring systems defined for the contact pairs of particles.

The contact force between two particles $\mathbf{F}$ can be deomposed into normal and tangential components, $\mathbf{F}_n$ and $\mathbf{F}_T$, respectively

$$\mathbf{F} = \mathbf{F}_n + \mathbf{F}_T = F_n \mathbf{n} + \mathbf{F}_T \,, \tag{11}$$

where $\mathbf{n}$ is the unit vector normal to the particle surface at the contact point.

The contact forces F_n and $\mathbf{F}_T$ are obtained using a constitutive model formulated for the contact between two rigid spheres. In the present formulation rock materials are modelled using elastic perfectly brittle model of contact interaction, where we assume initial bonding for the neighbouring particles. These bonds can be broken under load allowing us to simulate initiation and propagation of material fracture. Contact laws for the normal and tangential direction for the elastic perfectly brittle model are shown in figure 2. When two particles are

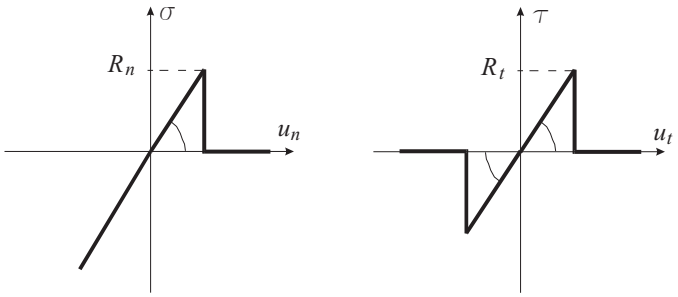

Figure 2: Force–displacement relationships for the elastic perfectly brittle model: a) in the normal direction, b) in the tangential direction

bonded the contact forces in both normal and tangential directions are calculated from the linear constitutive relationships:

$$F_n = k_n u_n \,, \tag{12}$$

$$\|\mathbf{F}_T\| = k_t \|\mathbf{u}_t\| \,, \tag{13}$$

where: k_n — interface stiffness in the normal direction, k_t — interface stiffness in the tangential direction, u_n — normal relative displacement, $\mathbf{u}_t$ — tangential relative displacement.

The tensile and shear contact forces are limited by the tensile and shear interface strengths, R_n and R_t, respectively:

$$F_n \leq R_n \,, \tag{14}$$

$$\|\mathbf{F}_t\| \leq R_t \,. \tag{15}$$

Cohesive bonds are broken instantaneously when the interface strength is exceeded either by the tangential contact force or by the tensile contact force.

In the absence of cohesion the normal contact force can be compressive only ($F_n \leq 0$) and tangential contact force can be nonzero due to friction. In the present formulation the Coulomb model of friction is used.

A quasi-static state of equilibrium of the assembly of particles can be achieved by application of adequate damping. Damping is necessary to dissipate kinetic energy. Damping terms $\mathbf{F}_i^{\mathrm{damp}}$ and $\mathbf{T}_i^{\mathrm{damp}}$ are added to equations of motion (57) and (58)

$$m_i\ddot{\mathbf{u}}_i = \mathbf{F}_i + \mathbf{F}_i^{\mathrm{damp}}, \tag{16}$$

$$I_i\dot{\boldsymbol{\omega}}_i = \mathbf{T}_i + \mathbf{T}_i^{\mathrm{damp}}. \tag{17}$$

Damping implemented used in the present work is of non-viscous type and is given by:

$$\mathbf{F}_i^{\mathrm{damp}} = -\alpha^t\|\mathbf{F}_i\|\frac{\dot{\mathbf{u}}_i}{\|\dot{\mathbf{u}}_i\|}, \tag{18}$$

$$\mathbf{T}_i^{\mathrm{damp}} = -\alpha^r\|\mathbf{T}_i\|\frac{\boldsymbol{\omega}_i}{\|\boldsymbol{\omega}_i\|}. \tag{19}$$

where α^t and α^r, are respective damping constants for translational and rotational motion.

1.3 Determination of rock model parameters

Determination of rock model parameters is the first step in our simulation of rock cutting process. A set of micromechanical parameters has to be established to model required macroscopic properties of the rock material which will be considered in rock cutting simulation.

The most important macroscopic properties are Young modulus E, Poisson ratio ν and compressive and tensile strengths, σ_c and σ_t, respectively. Microscopic parameters are, in turn, all the constitutive model parameters governing the interaction between a pair of particles: the normal and tangential stiffness k_n and k_T, the interface strengths in the normal and tangential directions, R_t and R_t, respectively, as well as the Coulomb friction coefficient μ.

Macroscopic material properties have been determined by laboratory tests, unconfined compression test and indirect tension (Brazilian) test, performed in the laboratory of Sandvik Mining and Construction GmbH [1] (Zeltweg, Austria). Numerical simulation of these tests will allow us to determine the microscopic constitutive parameters for a material sample modelled with discrete elements yielding the macroscopic properties of the real rock material. The averaged parameters from laboratory tests have been taken as the macroscopic properties of the studied rock as follows: Young modulus $E = 18690$ MPa, Poisson ratio $\nu = 0.23$, unconfined compression strength $\sigma_c = 127.8$ MPa, and tensile strength $\sigma_t = 12.3$ MPa.

1.3.1 *Simulation of unconfined compression test*

Figure 3 shows the unconfined compression test carried out in the laboratory of Sandvik Mining and Construction. Rock samples of equal height and diameter of 50 mm are used in the testing procedure adopted in this laboratory. Figure 3 demonstrates failure mode of the rock sample under compressive load.

Figure 4 presents a 2D material sample prepared for testing. A material sample of 50×50 mm is represented by an assembly of randomly compacted 4979 discs of radii 0.262–0.653 mm. It is shown in [7] that preparing a well-connected densely packed irregular assembly of particles is the key to successful simulation with discrete elements. Compaction of the particle assembly shown in Fig. 4 is characterized by a porosity of 13%.

The loading has been introduced under kinematic control by prescribing the motion of rigid plates pressing on the top and bottom of the sample. The deformation in the x direction was

[1] Former VOEST-Alpine Bergtechnik GmbH.

a) b)

Figure 3: Unconfined compression test: a) sample before the failure, b) after the failure of the rock sample

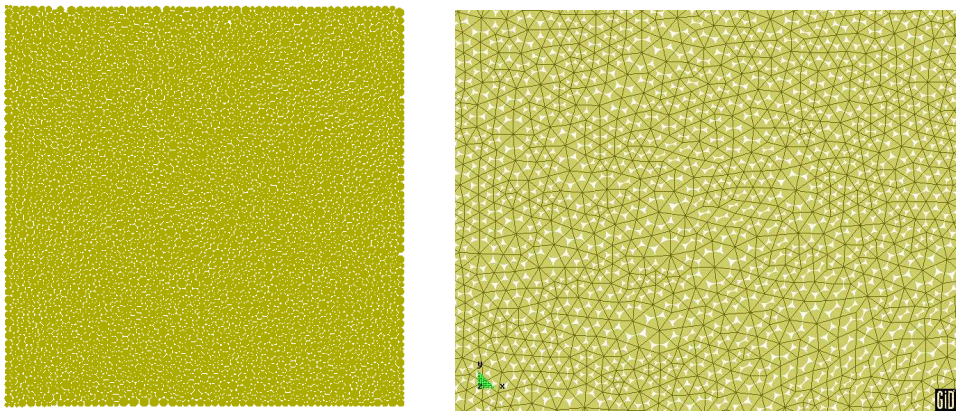

a) b)

Figure 4: Numerical model of unconfined compression test: a) discrete element model of the rock sample, b) detail of the model with contact bonds

free. The velocity of the wall displacement was 1 mm/s which was found to be sufficiently low to obtain quasi-static loading.

Using the methodology developed in [7] assuming undimensional relationships relating the micromechanical parameters to macroscopic properties the following set of micromechanical parameters has been found: contact stiffness in the normal direction $k_n = 1.61129 \cdot 10^{10}$ Pa, contact stiffness in the tangential direction $k_T = 0.3222 \cdot 10^{10}$ Pa, Coulomb friction coefficient $\mu = 0.839$ and cohesive bond strengths in the normal and tangential direction, $R_n = R_T = 0.29 \cdot 10^5$ N/m.

The failure evolution of the specimen obtained in the simulation with theses parameters is shown in Fig. 5. Comparison of Figs. 5 and 3 shows that numerical analysis yields a failure mode similar to that observed in experiments for brittle rocks. The stress-strain relationship shown in Fig. 6. It is similar to the stress-strain curves obtained in laboratory.

The theoretical macroscopic parameters obtained in the numerical simulation of unconfined compression test are as follows: Young modulus $E = 18000$ MPa, Poisson ratio $\nu = 0.20$, unconfined compression strength $\sigma_c = 116$ MPa.

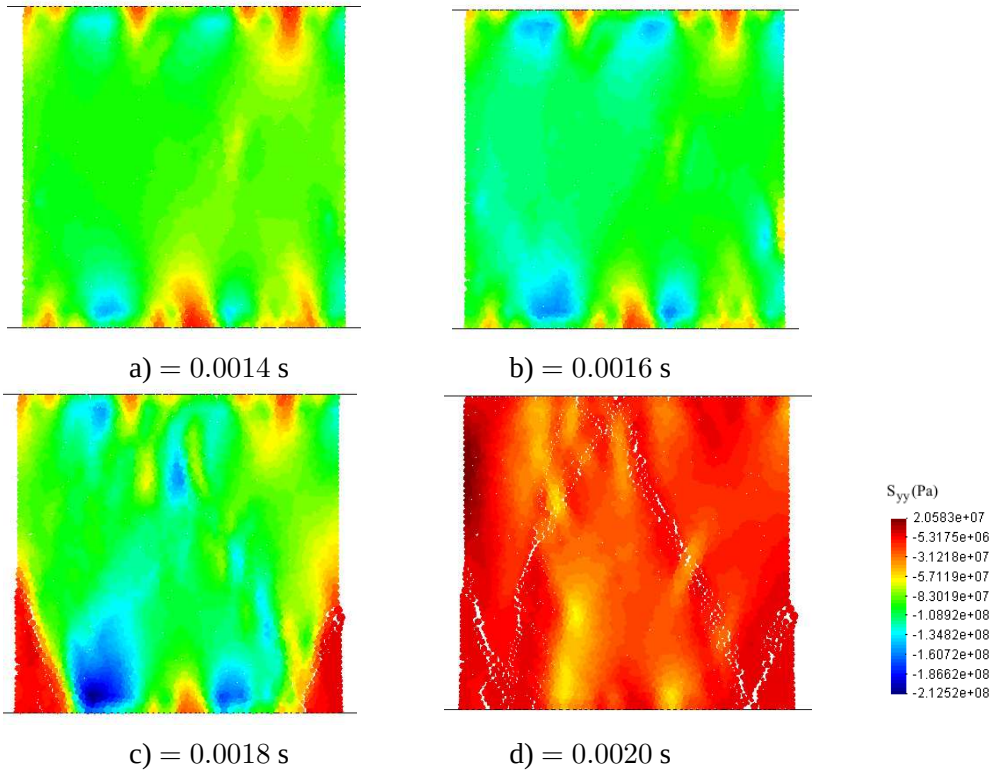

Figure 5: Simulation of unconfined compression test – failure evolution with distribution of stress along the loading direction

1.3.2 *Simulation of indirect tension (Brazilian) test*

Tensile strength of rocks is obtained experimentally from indirect tension (Brasilian) test. In the laboratory of Sandvik Mining and Construction cylindrical samples of diameter of 50 mm and height (length) of 25 mm have been used. Laboratory set-up and sample failure are shown in Fig. 7. The failure mode obtained in the analysis is shown in Figs. 8 and 9. Distributions of stresses in the direction parallel and normal to the loading directions shown in Figs. 8 and 9 are in a very good agreement with theoretical solutions [21].

The force–displacement relationship obtained in this simulation is plotted in Fig. 10. Taking the maximum force we find the tensile strength as:

$$\sigma_t = \frac{2P}{\pi LD} = \frac{2 \cdot 1.319 \cdot 10^6}{\pi \cdot 1 \cdot 0.05}\text{Pa} = 16.8\text{MPa} \tag{20}$$

which we accepted as satisfactorily agreeing with the experimental result, 12.3 MPa.

1.4 Modelling and simulation of rock cutting process

1.4.1 *Basic assumptions of rock cutting model*

A numerical model of the tool-rock system allowing us to simulate a process of rock cutting is developed within the framework of the spherical discrete element method (DEM). The main physical phenomenon considered is the interaction of the tool with a rock leading to failure of the rock characterized with discontinuous material behaviour. Rock material will be modelled using the discrete element method. The tool is considered rigid in our numerical model assuming that its stiffness is sufficient to produce rock failure and its deformation is irrelevant for the

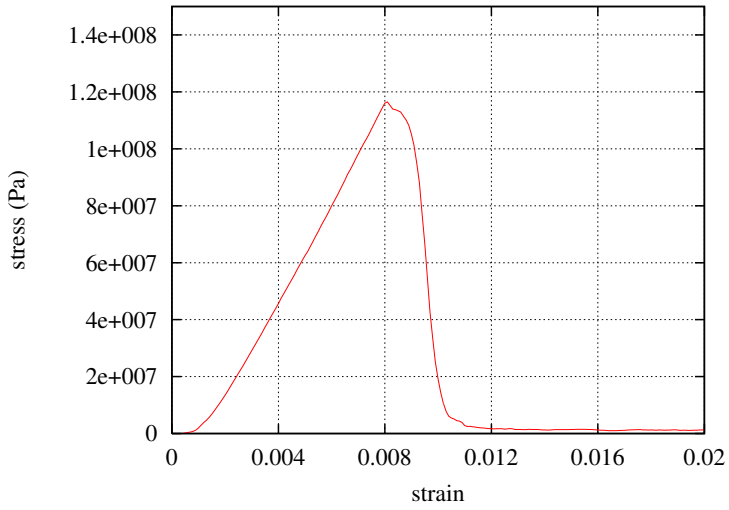

Figure 6: Simulation of unconfined compression test – stress–strain curve

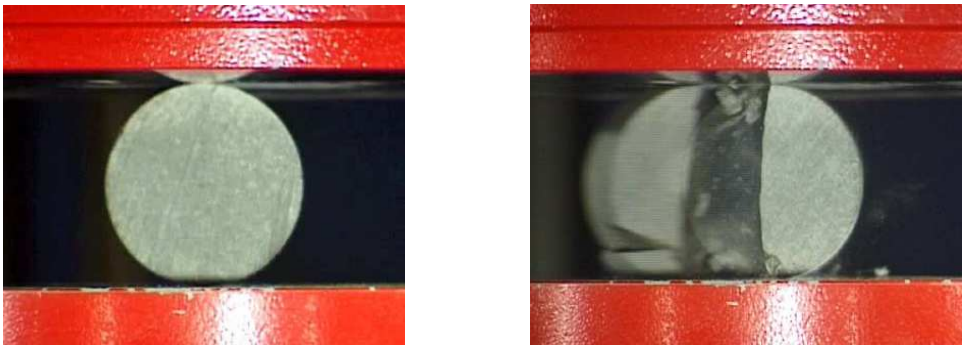

a) b)

Figure 7: Brazilian test: a) the rock sample before the failure, b) the rock sample after the failure

purposes of modelling of rock failure.

1.4.2 *Simulation of rock cutting laboratory test*

Validation of rock cutting model has been carried out comparing results of simulation of rock cutting with a single roadheader pick with experimental results obtained in a laboratory test performed in the laboratory of Sandvik Mining and Construction.

The scheme of the test rig is shown in Fig. 11a. A sandstone block is cut by a rotating tool. Mechanical properties of a rock are the same as those determined experimentally in section 1.3: compressive strength $\sigma_{\mathrm{c}} = 127$ MPa and tensile strength $\sigma_{\mathrm{t}} = 12$ MPa. Performance of rock cutting is shown in Fig. 11b. It can be seen splitting of chips typical for brittle rock cutting.

A numerical model developed for simulation of the rock cutting test is shown in Fig. 12a. The rock specimen is discretized using 30 750 cylindrical elements of radii $r = 1 - 1.5$ mm. Microscopic model parameters determined in the previous section have been scaled considering the change of the element size.

The cutting tool has been considered as rigid, allowing us to take into account its surface only. For the rock–tool interaction the following set of parameters has been assumed: $k_{\mathrm{n}} = k_{\mathrm{s}} = 5 \cdot 10^{10}$ MPa, $\mu = 0.5$. Non-viscous damping has been assumed taking the damping

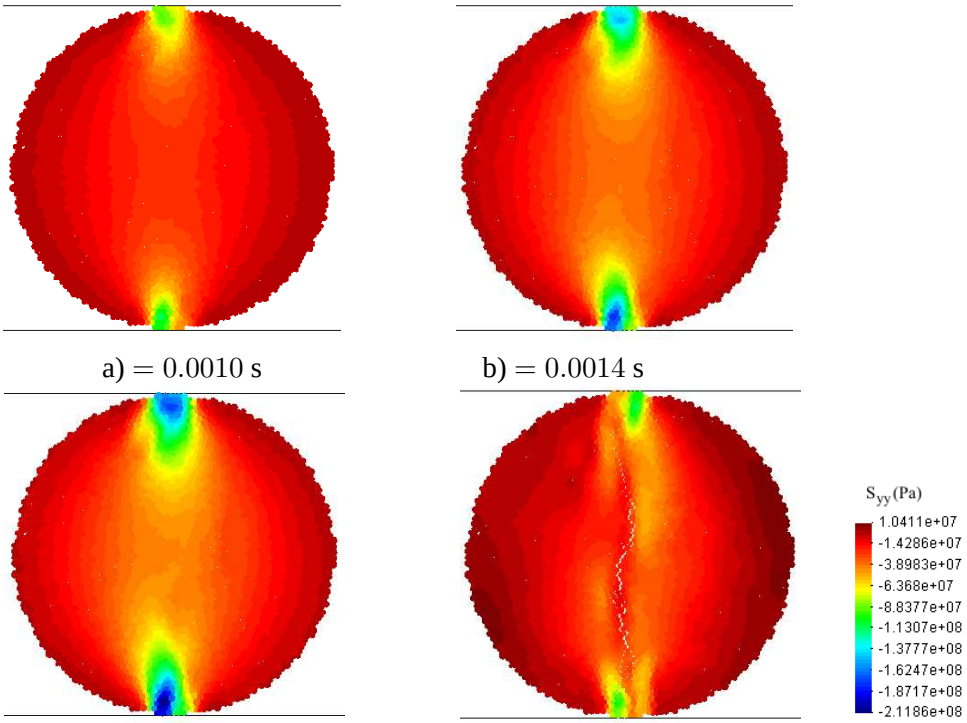

Figure 8: Simulation of Brazilian test – failure of the rock sample with distribution of stress in the direction along the loading

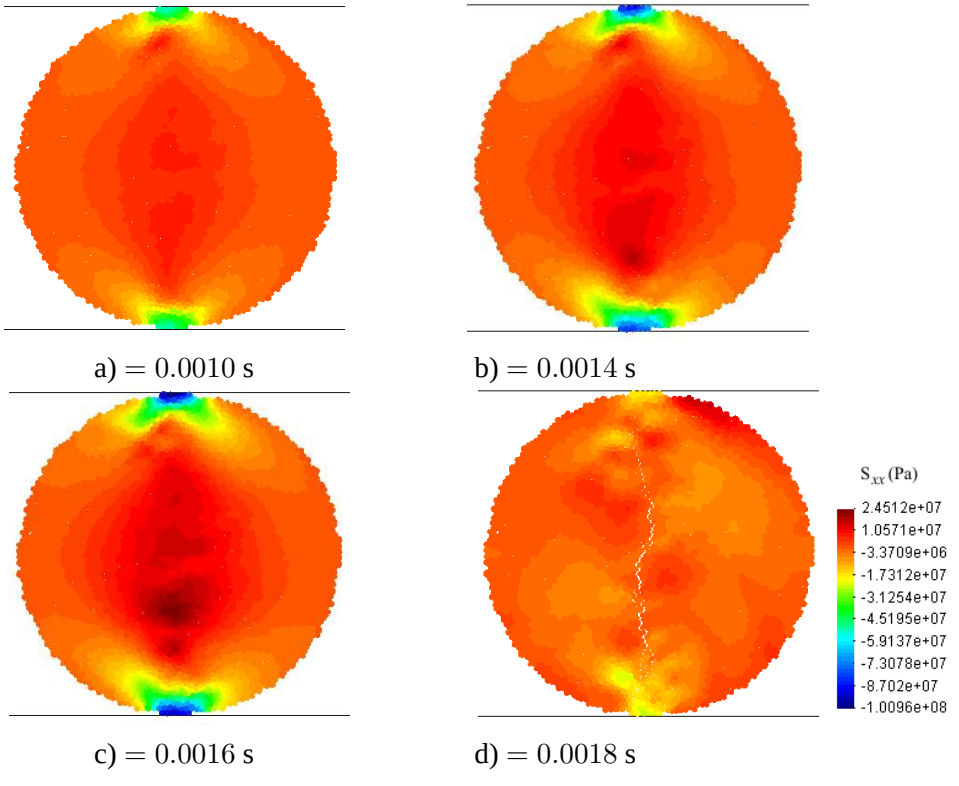

Figure 9: Simulation of Brazilian test – failure of the rock sample with distribution of stress in the direction normal to the loading

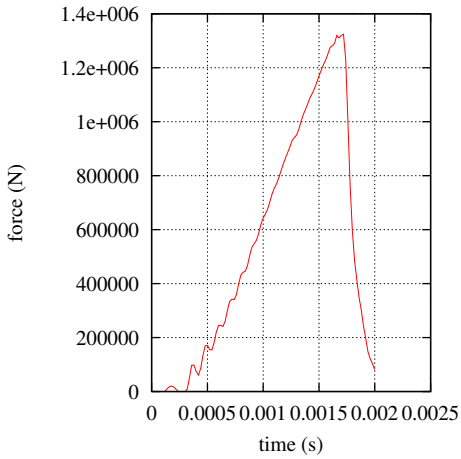

Figure 10: Simulation of the Brazilian test – stress–displacement curve

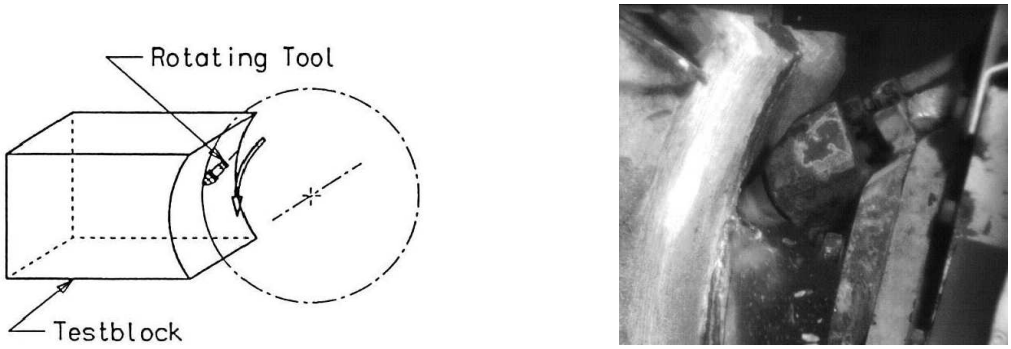

a) b)

Figure 11: Experimental validation of rock cutting: a) scheme of the test rig b) rock cutting test (laboratory of Sandvik Mining and Construction GmbH, Zeltweg, Austria)

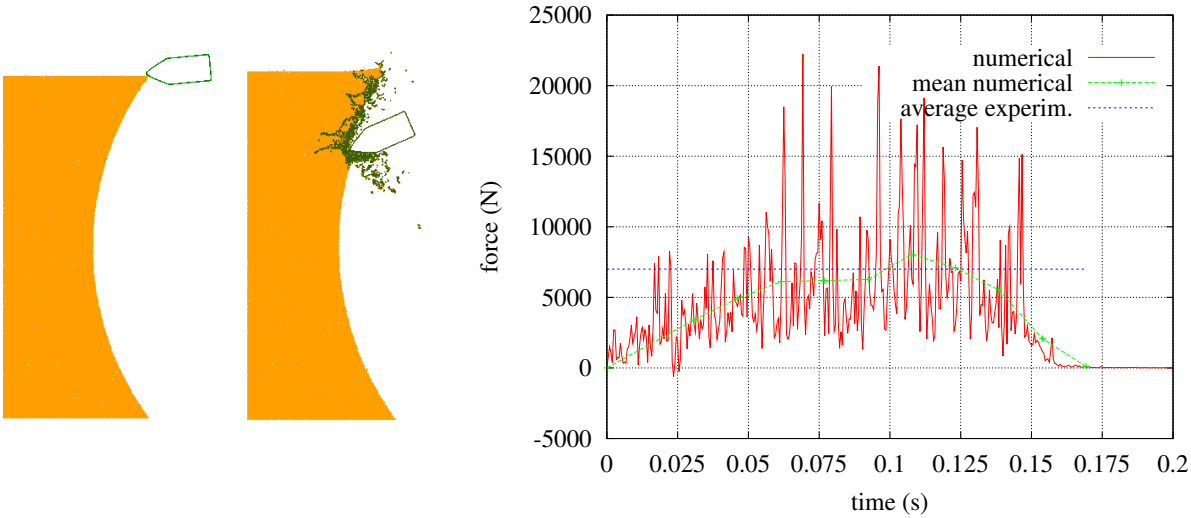

a) b) c)

Figure 12: Numerical simulation of rock cutting: a) numerical model, b) failure mode during rock cutting b) cutting force variation

factors $\alpha^{\mathrm{nvt}} = \alpha^{\mathrm{nvr}} = 0.2$.

Figure 12b shows the rock failure mode obtained in the simulation. It can be noticed a good enough agreement with the failure observed in the laboratory test. Figure 12c shows variation of the cutting force obtained in the numerical simulation. Numerical and experimental average forces have been compared in Fig. 12c. The mean cutting force from the numerical analysis agrees quite well with the average experimental force (about 7000 kN).

2 COUPLED DISCRETE/FINITE ELEMENT MODELLING OF UNDERGROUND EXCAVATION

2.1 Introduction

Discrete element method usually requires use of large number of elements which leads to long computation times. Continuous material is usually modelled more efficiently using the finite element method. Combining these two methods in one model of rock cutting allows us to take advantages of each method. Discrete elements are used only in a portion of the analysed domain where material fracture occurs, while outside the DEM subdomain finite elements can be used.

2.2 Discrete element method formulation

The discrete element method formulation used in this work has been briefly reviewed in subsection . Let us rewrite translational and rotational equations of motion of discrete elements (57) and (58) in the global form for the whole assembly of discrete elements:

$$\mathbf{M}_{\mathrm{D}}\ddot{\mathbf{r}}_{\mathrm{D}} = \mathbf{F}_{\mathrm{D}} \tag{21}$$

$$\mathbf{J}_{\mathrm{D}}\dot{\boldsymbol{\Omega}}_{\mathrm{D}} = \mathbf{T}_{\mathrm{D}} \tag{22}$$

where $\mathbf{r}_{\mathrm{D}}$ is the position vector of the element centroid in a fixed (inertial) coordinate frame, $\boldsymbol{\Omega}_{\mathrm{D}}$ – angular velocity, $\mathbf{M}_{\mathrm{D}}$ – diagonal matrix with the element mass on the diagonal, $\mathbf{J}_{\mathrm{D}}$ – diagonal matrix with the element moment of inertia on the diagonal, $\mathbf{F}_{\mathrm{D}}$ – vector of resultant forces, and $\mathbf{T}_{\mathrm{D}}$ – vector of resultant moments about the element central axes. Vectors $\mathbf{F}_{\mathrm{D}}$ and $\mathbf{T}_{\mathrm{D}}$ are sums of all forces and moments applied to the element due to external load, contact interactions with neighbouring spheres and other obstacles, as well as forces resulting from damping in the system.

2.3 Finite element method formulation

In the present work the so-called explicit dynamic formulation of the finite element method is used. The explicit FEM is based on the solution of discretized equations of motion written in the current configuration in the following form:

$$\mathbf{M}_{\mathrm{F}}\ddot{\mathbf{r}}_{\mathrm{F}} = \mathbf{F}_{\mathrm{F}}^{\mathrm{ext}} - \mathbf{F}_{\mathrm{F}}^{\mathrm{int}} \tag{23}$$

where $\mathbf{M}_{\mathrm{F}}$ is the mass matrix, $\mathbf{r}_{\mathrm{F}}$ is the vector of nodal displacements, $\mathbf{F}_{\mathrm{F}}^{\mathrm{ext}}$ and $\mathbf{F}_{\mathrm{F}}^{\mathrm{int}}$ are the vectors of external loads and internal forces, respectively. The element internal force vector is calculated according to the following relationship:

$$\mathbf{F}_{\mathrm{F}}^{\mathrm{int}} = \int_V \mathbf{B}^{\mathrm{T}}\boldsymbol{\sigma}\,\mathrm{d}V \tag{24}$$

where $\boldsymbol{\sigma}$ is the Cauchy stress tensor, and $\mathbf{B}$ is the linear strain-displacement operator matrix. Similarly to the DEM algorithm, the central difference scheme is used for time integration of Eq. (23).

2.4 Coupling the discrete and finite element methods

2.4.1 *Problem formulation*

In the combined DEM/FEM models the DEM and FEM can be applied in disjoint domains or can be employed in different subdomains of the same body. In the former case the DEM

equations (21)–(22) are coupled with the explicit FEM equations (23) by the contact forces resulting from interaction between discrete elements and boundaries of subdomains discretized with finite elements. Thanks to the same structure of the equations (21)–(22) and (23) the same solution scheme can be adopted. This coupling algorithm has been presented in [12]. Here the coupling has been extended to the case in which DEM and FEM used in different subdomains of the same body. The coupling of DEM and FEM used in this case is provided by additional kinematical constraints. Interface discrete elements are constrained by the displacement field of overlapping interface finite elements. The constraints are imposed by the Lagrange multiplier or penalty method.

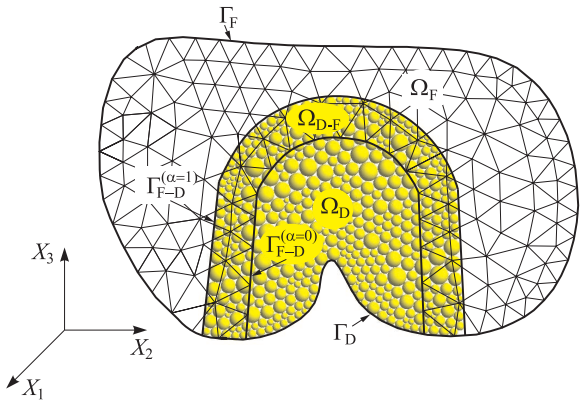

Figure 13: Hybrid DEM/FEM model with transitory zone

Motion of a deformable body occupying the domain Ω with the boundary Γ will be considered. Two different subdomains will be distinguished in the domain Ω (Fig. 13), Ω_F – discretized with finite elements and Ω_D – modelled with discrete elements

$$\Omega = \Omega_{\text{F}} \cup \Omega_{\text{D}} \tag{25}$$

The subdomains Ω_F and Ω_D are not disjoint – they can overlap each other. The common part of the subdomains Ω_F and Ω_D

$$\Omega_{\text{D-F}} = \Omega_{\text{F}} \cap \Omega_{\text{D}} \neq \emptyset \tag{26}$$

is the part where both discretization types are used. This idea follows that used for molecular dynamics coupling with a continous model in [20]. The virtual work in the domain Ω will be written as linear combination of the virtual work δW_F due to the finite element contribution and δW_D yielded by the discrete element part of the model

$$\delta W = \alpha \delta W_{\text{F}} + (1-\alpha)\delta W_{\text{D}} \tag{27}$$

where the function α is defined in the following way:

$$\alpha(\boldsymbol{x}) = \begin{cases} 0 & \text{for } \boldsymbol{x} \in \Omega_{\text{D}} \setminus \Omega_{\text{D-F}} \\ \dfrac{g(\boldsymbol{x})}{L(\boldsymbol{x})} & \text{for } \boldsymbol{x} \in \Omega_{\text{D-F}} \\ 1 & \text{for } \boldsymbol{x} \in \Omega_{\text{F}} \setminus \Omega_{\text{D-F}} \end{cases} \tag{28}$$

In the transition zone $\Omega_{\text{D-F}}$ the value of function α varies linearly from zero on the surface $\Gamma_{\text{D-F}}^{(\alpha=0)}$ to unity on the surface $\Gamma_{\text{D-F}}^{(\alpha=1)}$ (Fig. 14). The surface $\Gamma_{\text{D-F}}^{(\alpha=0)}$ separates the domain of

mixed discrete–continuous modelling from the domain where the discrete element method is used only:

$$\Gamma_{\text{D-F}}^{(\alpha=0)} = \Gamma_{\text{F}} \cap \Omega_{\text{D}} \,. \tag{29}$$

The surface $\Gamma_{\text{D-F}}^{(\alpha=1)}$, in turn, separates the transition zone from the domain of continuous mod-

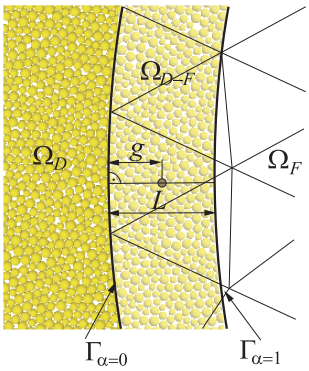

Figure 14: Geometrical illustration of the parameters defining the scaling function α

elling discretized with finite elements:

$$\Gamma_{\text{D-F}}^{(\alpha=1)} = \Gamma_{\text{D}} \cap \Omega_{\text{F}} \,. \tag{30}$$

Definition of the functions $g(\boldsymbol{x})$ and $L(\boldsymbol{x})$ is shown graphically in Fig. 14. The function $g(\boldsymbol{x})$ is defined as the shortest distance from the point $\boldsymbol{x} \in \Omega_{D-F}$ to the boundary of the overlap region $\Gamma_{\text{D-F}}^{(\alpha=0)}$:

$$g(\boldsymbol{x}) = || \, \bar{\boldsymbol{x}}^{(0)} - \boldsymbol{x}|| \tag{31}$$

where $\boldsymbol{x} \in \Omega_{\text{D-F}}$, and

$$\bar{\boldsymbol{x}}^{(0)} \in \Gamma_{\text{D-F}}^{(\alpha=0)} : \; || \, \bar{\boldsymbol{x}}^{(0)} - \boldsymbol{x}|| = \min_{\boldsymbol{x}^{(0)} \in \Gamma_{\text{D-F}}^{(\alpha=0)}} ||\boldsymbol{x}^{(0)} - \boldsymbol{x}|| \tag{32}$$

The function $L(\boldsymbol{x})$ is the width of the overlap zone measured along the vector $\bar{\boldsymbol{x}}^{(0)} - \boldsymbol{x}$.

Finite element discretization employed in the subdomain Ω_{F} allows us to express the displacement, velocity and acceleration fields in the discretized region, $\boldsymbol{u}_{\text{F}}$, $\dot{\boldsymbol{u}}_{\text{F}}$ and $\ddot{\boldsymbol{u}}_{\text{F}}$, respectively, in terms of shape functions $\mathbf{N}$ and nodal displacements, velocities and accelarations, $\mathbf{r}_{\text{F}}$, $\dot{\mathbf{r}}_{\text{F}}$ and $\ddot{\mathbf{r}}_{\text{F}}$.

In the subdomain Ω_{D} discrete model is employed. A set of n_{de} discrete elements $D = \{d_i\}$, $i = 1, n_{de}$ is introduced. Domain occupied by the discrete elements is a subset of the set Ω_{D}

$$\tilde{\Omega}_{\text{D}} = \bigcup_{i=1}^{i=n_{\text{de}}} d_i \subset \Omega_{\text{D}} \tag{33}$$

Configuration and motion of the discrete elements are described by the vectors of translational displacements, $\mathbf{r}_D$, translational and rotational velocities, $\dot{\mathbf{r}}_{\text{D}}$ and $\boldsymbol{\Omega}_{\text{D}}$, and translational and rotational accelerations, $\ddot{\mathbf{r}}_{\text{D}}$ and $\dot{\boldsymbol{\Omega}}_{\text{D}}$, respectively.

2.4.2 *Kinematic constraints coupling the DEM and FEM subdomains*

The subdomains Ω_F and Ω_D are coupled in the common transition zone $\Omega_{\text{D-F}}$. Coupling is provided by additional kinematic constraints resulting from the assumption that the discrete elements forming the set

$$D_{\text{D-F}} = \{d_i : \boldsymbol{x}_{d_i} \in \Omega_{\text{D-F}}\} \tag{34}$$

are constrained kinematically by the finite element discretization

$$\chi_i = \boldsymbol{x}_{d_i} - \boldsymbol{x}_{\text{F}} = \boldsymbol{u}_{d_i} - \boldsymbol{u}_{\text{F}}(\boldsymbol{x}_{\text{F}}) = \boldsymbol{0}\,, \tag{35}$$

$$\delta\chi_i = \delta\boldsymbol{u}_{d_i} - \sum_{j=1}^{n_w} N_j(\boldsymbol{x}_{\text{F}})\delta\boldsymbol{u}_{\text{F}j} = \boldsymbol{0}\,, \tag{36}$$

$$\dot{\chi}_i = \dot{\boldsymbol{u}}_{d_i} - \sum_{j=1}^{n_w} N_j(\boldsymbol{x}_{\text{F}})\dot{\boldsymbol{u}}_{\text{F}j} = \boldsymbol{0}\,, \tag{37}$$

$$\ddot{\chi}_i = \ddot{\boldsymbol{u}}_{d_i} - \sum_{j=1}^{n_w} N_j(\boldsymbol{x}_{\text{F}})\ddot{\boldsymbol{u}}_{\text{F}j} = \boldsymbol{0} \tag{38}$$

Making use of the split of the global vectors of displacements, velocities and accelerations $\mathbf{r}_{\text{D}}$, $\dot{\mathbf{r}}_{\text{D}}$ and $\ddot{\mathbf{r}}_{\text{D}}$, into the unconstrained parts $\mathbf{r}_{\text{DU}}$, $\dot{\mathbf{r}}_{\text{DU}}$ and $\ddot{\mathbf{r}}_{\text{DU}}$, and constrained ones $\mathbf{r}_{\text{DC}}$, $\dot{\mathbf{r}}_{\text{DC}}$ i $\ddot{\mathbf{r}}_{\text{DC}}$, kinematic relationships (35)–(38) can be written jointly for all the constrained discrete elements in the matrix notation as follows:

$$\boldsymbol{\chi} = \mathbf{r}_{\text{DC}} - \mathbf{N}\mathbf{r}_{\text{F}} = \mathbf{0}\,, \tag{39}$$

$$\delta\boldsymbol{\chi} = \delta\mathbf{r}_{\text{DC}} - \mathbf{N}\delta\mathbf{r}_{\text{F}} = \mathbf{0}\,, \tag{40}$$

$$\dot{\boldsymbol{\chi}}_i = \dot{\mathbf{r}}_{\text{DC}} - \mathbf{N}\dot{\mathbf{r}}_{\text{F}} = \mathbf{0}\,, \tag{41}$$

$$\ddot{\boldsymbol{\chi}}_i = \ddot{\mathbf{r}}_{\text{DC}} - \mathbf{N}\ddot{\mathbf{r}}_{\text{F}} = \mathbf{0}\,. \tag{42}$$

Additional kinematic constraints (40) will be imposed by two alternative methods:

- Lagrange multipliers method,
- penalty function method.

2.4.3 *Coupled equations of motion – Lagrange multipliers method*

The principle of virtual work for the coupled FEM/DEM system with constraints (39) included by means of the Lagrange multipliers method can be written in the following form:

$$\begin{aligned}\delta\mathbf{r}_{\text{F}}^{\text{T}}\left(\bar{\mathbf{M}}_{\text{F}}\ddot{\mathbf{r}}_{\text{F}} + \bar{\mathbf{F}}_{\text{F}}^{\text{int}} - \bar{\mathbf{F}}_{\text{F}}^{\text{ext}}\right) + \delta\mathbf{r}_{\text{D}}^{\text{T}}\left(\bar{\mathbf{M}}_{\text{D}}\ddot{\mathbf{r}}_{\text{D}} - \bar{\mathbf{F}}_{\text{D}}\right)\\ +\delta\boldsymbol{\Phi}_{\text{D}}^{\text{T}}\left(\bar{\mathbf{J}}_{\text{D}}\dot{\boldsymbol{\Omega}}_{\text{D}} - \bar{\mathbf{T}}_{\text{D}}\right) + \delta\boldsymbol{\chi}^{\text{T}}\boldsymbol{\lambda} = 0\end{aligned} \tag{43}$$

where $\boldsymbol{\lambda}$ is the vector of unknown Lagrange multipliers, $\delta\mathbf{r}_{\text{F}}$ and $\delta\mathbf{r}_{\text{D}}$ are kinematically admissible virtual displacements, $\delta\boldsymbol{\Phi}_{\text{D}}$ – elementary rotations. The global matrices $\bar{\mathbf{M}}_{\text{F}}$, $\bar{\mathbf{M}}_{\text{D}}$ and $\bar{\mathbf{J}}_{\text{D}}$, and vectors $\bar{\mathbf{F}}_{\text{F}}^{\text{int}}$, $\bar{\mathbf{F}}_{\text{F}}^{\text{ext}}$, $\bar{\mathbf{F}}_{\text{D}}$ and $\bar{\mathbf{T}}_{\text{D}}$ are assemebled from appropriate elemental matrices and vectors considering contributions from the finite element and discrete element parts according to the assumption expressed by Eq. (27):

$$\bar{\mathbf{f}}_e^{\text{int}} = \int_{\Omega_e} \alpha\mathbf{B}^{\text{T}}\sigma\,\mathrm{d}\Omega_e\,, \tag{44}$$

$$\bar{\mathbf{f}}_e^{\text{ext}} = \int_{\Omega_e} \alpha \mathbf{N}^{\mathrm{T}} \rho \mathbf{b} \, \mathrm{d}\Omega_e + \int_{\Gamma_e \cap \Gamma_\sigma} \alpha \mathbf{N}^{\mathrm{T}} \mathbf{t} \, \mathrm{d}\Gamma_e \,, \tag{45}$$

$$\bar{\mathbf{m}}_e = \int_{\Omega_e} \alpha \rho \mathbf{N}^{\mathrm{T}} \mathbf{N} \, \mathrm{d}\Omega_e \,, \tag{46}$$

$$\bar{\mathbf{f}}_{d_i} = (1-\alpha)\mathbf{f}_{d_i} \,, \tag{47}$$

$$\bar{\mathbf{m}}_{d_i} = (1-\alpha)\mathbf{m}_{d_i} \,, \tag{48}$$

$$\bar{\mathbf{J}}_{d_i} = (1-\alpha)\mathbf{J}_{d_i} \,, \tag{49}$$

$$\bar{\mathbf{T}}_{d_i} = (1-\alpha)\mathbf{T}_{d_i} \,. \tag{50}$$

Taking into account the split $\mathbf{r}_{\text{D}} = \{\mathbf{r}_{\text{DU}}, \mathbf{r}_{\text{DC}}\}^{\mathrm{T}}$ and the explicit form of the constraint equation (40), equation (43) can be written in the following form:

$$\begin{aligned} &\delta\mathbf{r}_{\text{F}}^{\mathrm{T}} \left(\bar{\mathbf{M}}_{\text{F}} \ddot{\mathbf{r}}_{\text{F}} + \bar{\mathbf{F}}_{\text{F}}^{\text{int}} - \bar{\mathbf{F}}_{\text{F}}^{\text{ext}} \right) \\ &+\delta\mathbf{r}_{\text{DU}}^{\mathrm{T}} \left(\bar{\mathbf{M}}_{\text{DU}} \ddot{\mathbf{r}}_{\text{DU}} - \bar{\mathbf{F}}_{\text{DU}} \right) + \delta\mathbf{r}_{\text{DC}}^{\mathrm{T}} \left(\bar{\mathbf{M}}_{\text{DC}} \ddot{\mathbf{r}}_{\text{DC}} - \bar{\mathbf{F}}_{\text{DC}} \right) \\ &+\delta\boldsymbol{\Phi}_{\text{D}}^{\mathrm{T}} \left(\bar{\mathbf{J}}_{\text{D}} \dot{\boldsymbol{\Omega}}_{\text{D}} - \bar{\mathbf{T}}_{\text{D}} \right) - \delta\mathbf{r}_{\text{F}}^{\mathrm{T}} \mathbf{N}^{\mathrm{T}} \boldsymbol{\lambda} + \delta\mathbf{r}_{\text{DC}}^{\mathrm{T}} \boldsymbol{\lambda} = 0 \,. \end{aligned} \tag{51}$$

Based on the requirement that equation (51) must be satisfied for arbitrary admissible variations, and with addition of the the relationship for accelerations (42) the following equation set is obtained for the coupled system:

$$\begin{bmatrix} \bar{\mathbf{M}}_{\text{F}} & \mathbf{0} & \mathbf{0} & \mathbf{0} & -\mathbf{N}^{\mathrm{T}} \\ \mathbf{0} & \bar{\mathbf{M}}_{\text{DU}} & \mathbf{0} & \mathbf{0} & \mathbf{0} \\ \mathbf{0} & \mathbf{0} & \bar{\mathbf{M}}_{\text{DC}} & \mathbf{0} & \mathbf{I} \\ \mathbf{0} & \mathbf{0} & \mathbf{0} & \bar{\mathbf{J}}_{\text{D}} & \mathbf{0} \\ -\mathbf{N} & \mathbf{0} & \mathbf{I} & 0 & \mathbf{0} \end{bmatrix} \begin{Bmatrix} \ddot{\mathbf{r}}_{\text{F}} \\ \ddot{\mathbf{r}}_{\text{DU}} \\ \ddot{\mathbf{r}}_{\text{DC}} \\ \dot{\boldsymbol{\Omega}}_{\text{D}} \\ \boldsymbol{\lambda} \end{Bmatrix} = \begin{Bmatrix} \bar{\mathbf{F}}_{\text{F}}^{\text{ext}} - \bar{\mathbf{F}}_{\text{F}}^{\text{int}} \\ \bar{\mathbf{F}}_{\text{DU}} \\ \bar{\mathbf{F}}_{\text{DC}} \\ \bar{\mathbf{T}}_{\text{D}} \\ \mathbf{0} \end{Bmatrix} . \tag{52}$$

The vector of unknowns in Eq. (52) contains kinematic-type unknowns as well as force-type unknowns – Lagrange multiupliers. Equations (52) can be solved directly with respect to these unknowns using an adequate integration scheme. An alternative solution scheme consists in elimination of Lagrange multiupliers $\boldsymbol{\lambda}$ and dependent variables $\mathbf{r}_{\text{DC}}$ prior to integration. Performing some algebraic transformations equation (52) yields the following reduced equation set:

$$\begin{aligned} \left(\bar{\mathbf{M}}_{\text{F}} + \mathbf{N}^{\mathrm{T}} \bar{\mathbf{M}}_{\text{DC}} \mathbf{N} \right) \ddot{\mathbf{r}}_{\text{F}} &= \bar{\mathbf{F}}_{\text{F}}^{\text{ext}} - \bar{\mathbf{F}}_{\text{F}}^{\text{int}} + \mathbf{N}^{\mathrm{T}} \bar{\mathbf{F}}_{\text{DC}} \,, \\ \bar{\mathbf{M}}_{\text{DU}} \ddot{\mathbf{r}}_{\text{DU}} &= \bar{\mathbf{F}}_{\text{DU}} \,, \\ \bar{\mathbf{J}}_{\text{D}} \dot{\boldsymbol{\Omega}}_{\text{D}} &= \bar{\mathbf{T}}_{\text{D}} \,, \end{aligned} \tag{53}$$

which can be integrated in time using the standard central difference scheme.

2.4.4 *Coupled equations of motion – penalty function method*

The principle of virtual work for the coupled FEM/DEM system with constraints (39) included by means of the penalty function method can be written in the following form:

$$\begin{aligned} &\delta\mathbf{r}_{\text{F}}^{\mathrm{T}} \left(\bar{\mathbf{M}}_{\text{F}} \ddot{\mathbf{r}}_{\text{F}} + \bar{\mathbf{F}}_{\text{F}}^{\text{int}} - \bar{\mathbf{F}}_{\text{F}}^{\text{ext}} \right) + \delta\mathbf{r}_{\text{D}}^{\mathrm{T}} \left(\bar{\mathbf{M}}_{\text{D}} \ddot{\mathbf{r}}_{\text{D}} - \bar{\mathbf{F}}_{\text{D}} \right) \\ &+\delta\boldsymbol{\Phi}_{\text{D}}^{\mathrm{T}} \left(\bar{\mathbf{J}}_{\text{D}} \dot{\boldsymbol{\Omega}}_{\text{D}} - \bar{\mathbf{T}}_{\text{D}} \right) + \delta\boldsymbol{\chi}^{\mathrm{T}} \mathbf{k}_{\text{DF}} \boldsymbol{\chi} = 0 \end{aligned} \tag{54}$$

where $\mathbf{k}_{\mathrm{DF}}$ is the diagonal matrix containing on its diagonal the values of the discrete penalty function, and global matrices $\bar{\mathbf{M}}_{\mathrm{F}}$, $\bar{\mathbf{M}}_{\mathrm{D}}$ and $\bar{\mathbf{J}}_{\mathrm{D}}$, and global vectors $\bar{\mathbf{F}}_{\mathrm{F}}^{\mathrm{int}}$, $\bar{\mathbf{F}}_{\mathrm{F}}^{\mathrm{ext}}$, $\bar{\mathbf{F}}_{\mathrm{D}}$ and $\bar{\mathbf{T}}_{\mathrm{D}}$ are obtained by aggregation of adequate elemental matrices and vectors taking into account appropriate contributions from the discrete and finite element parts to the virtual work in agreement with Eq. (27) according to equations (44)–(48). Taking into account the split $\mathbf{r}_{\mathrm{D}} = \{\mathbf{r}_{\mathrm{DU}}, \mathbf{r}_{\mathrm{DC}}\}^{\mathrm{T}}$ and the explicit form of the constraint equation (40), equation (54) can be written in the following form:

$$\begin{aligned}
&\delta\mathbf{r}_{\mathrm{F}}^{\mathrm{T}}\left(\bar{\mathbf{M}}_{\mathrm{F}}\ddot{\mathbf{r}}_{\mathrm{F}} + \bar{\mathbf{F}}_{\mathrm{F}}^{\mathrm{int}} - \bar{\mathbf{F}}_{\mathrm{F}}^{\mathrm{ext}}\right) + \delta\mathbf{r}_{\mathrm{DU}}^{\mathrm{T}}\left(\bar{\mathbf{M}}_{\mathrm{DU}}\ddot{\mathbf{r}}_{\mathrm{DU}} - \bar{\mathbf{F}}_{\mathrm{DU}}\right)\\
&\quad+\delta\mathbf{r}_{\mathrm{DC}}^{\mathrm{T}}\left(\bar{\mathbf{M}}_{\mathrm{DC}}\ddot{\mathbf{r}}_{\mathrm{DC}} - \bar{\mathbf{F}}_{\mathrm{DC}}\right) + \delta\boldsymbol{\Phi}_{\mathrm{D}}^{\mathrm{T}}\left(\bar{\mathbf{J}}_{\mathrm{D}}\dot{\boldsymbol{\Omega}}_{\mathrm{D}} - \bar{\mathbf{T}}_{\mathrm{D}}\right)\\
&\quad-\delta\mathbf{r}_{\mathrm{F}}^{\mathrm{T}}\mathbf{N}^{\mathrm{T}}\mathbf{k}_{\mathrm{DF}}\boldsymbol{\chi} + \delta\mathbf{r}_{\mathrm{DC}}^{\mathrm{T}}\mathbf{k}_{\mathrm{DF}}\boldsymbol{\chi} = 0\,,
\end{aligned} \tag{55}$$

Based on the requirement that equation (55) must be satisfied for arbitrary admissible variations, and with addition of the the relationship for accelerations (42) the following equation set is obtained for the coupled system:

$$\begin{bmatrix}
\bar{\mathbf{M}}_{\mathrm{F}} & \mathbf{0} & \mathbf{0} & \mathbf{0}\\
\mathbf{0} & \bar{\mathbf{M}}_{\mathrm{DU}} & \mathbf{0} & \mathbf{0}\\
\mathbf{0} & \mathbf{0} & \bar{\mathbf{M}}_{\mathrm{DC}} & \mathbf{0}\\
\mathbf{0} & \mathbf{0} & \mathbf{0} & \bar{\mathbf{J}}_{\mathrm{D}}
\end{bmatrix}
\begin{Bmatrix}
\ddot{\mathbf{r}}_{\mathrm{F}}\\
\ddot{\mathbf{r}}_{\mathrm{DU}}\\
\ddot{\mathbf{r}}_{\mathrm{DC}}\\
\dot{\boldsymbol{\Omega}}_{\mathrm{D}}
\end{Bmatrix}
=
\begin{Bmatrix}
\bar{\mathbf{F}}_{\mathrm{F}}^{\mathrm{ext}} - \bar{\mathbf{F}}_{\mathrm{F}}^{\mathrm{int}} + \mathbf{N}^{\mathrm{T}}\mathbf{k}_{\mathrm{DF}}\boldsymbol{\chi}\\
\bar{\mathbf{F}}_{\mathrm{DU}}\\
\bar{\mathbf{F}}_{\mathrm{DC}} - \mathbf{k}_{\mathrm{DF}}\boldsymbol{\chi}\\
\bar{\mathbf{T}}_{\mathrm{D}}
\end{Bmatrix} \tag{56}$$

Equation (56) can be integrated in time using the standard central difference scheme.

2.5 Numerical examples

2.5.1 *Study of wave propagation across the DEM/FEM interface*

Wave propagation is a typical phenomenon observed in the dynamic solution of geomechanical problems modelled with discrete and/or finite element methods. The interface between the FEM and DEM subdomains can introduce an artificial internal boundary causing unrealistic wave reflections. Correct performance of the coupling method in the presence of wave propagation is shown in Fig. 15. The wave pulse travels from the DEM subdomain to the FEM one.

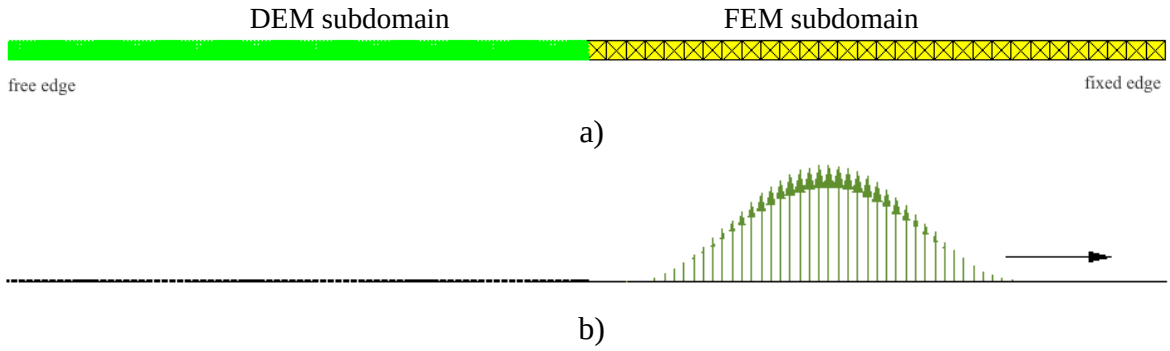

Figure 15: Wave propagation across the DEM/FEM interface: a) hybrid DEM/FEM model, b) wave pulse after passing the interface

2.5.2 *Simulation of rock cutting with a single pick of a roadheader cutter-head*

A process of rock cutting with a single pick of a roadheader cutter-head has been simulated using a discrete element method in [15]. The same example is analysed here using discrete and hybrid discrete/finite element models. In the hybrid DEM/FEM model discrete elements have been used in the part of rock mass subjected to fracture, while the other part have been discretized with finite elements. In both models the tool is considered rigid, assuming the elasticity of the tool is irrelevant for the purpose of modelling of rock fracture. Model parameters for the discrete element method have been determined in [16].

Figure 16 presents results of DEM simulation of rock cutting, and results of DEM/FEM simulation are shown in Fig. 17. The results presented have been obtained using the penalty

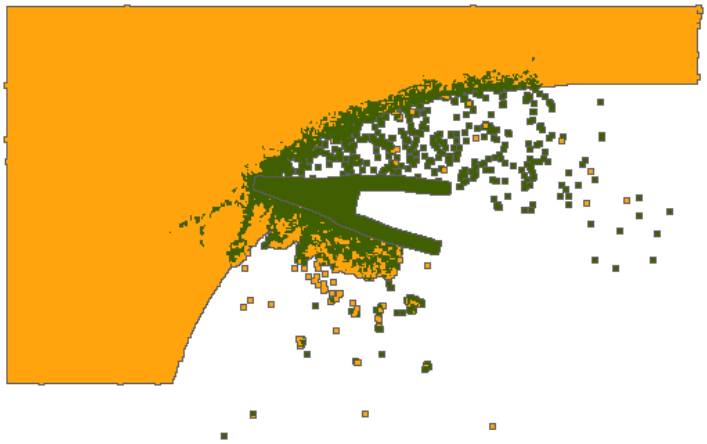

Figure 16: DEM simulation of rock cutting

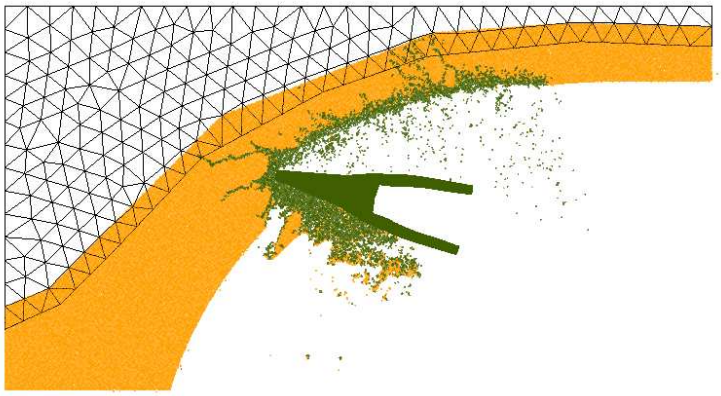

Figure 17: Combined DEM/FEM simulation of rock cutting

coupling method. Both models produce similar failures of rock during cutting. Cutting forces obtained using these two models are compared in Fig. 18. Both curves show oscillations typical for cutting of brittle rock. In both cases similar values of amplitudes are observed. Mean values of cutting forces agree very well. This shows that combined DEM/FEM simulation gives similar results to a DEM analysis, while being more efficient numerically – computation time has been reduced by half.

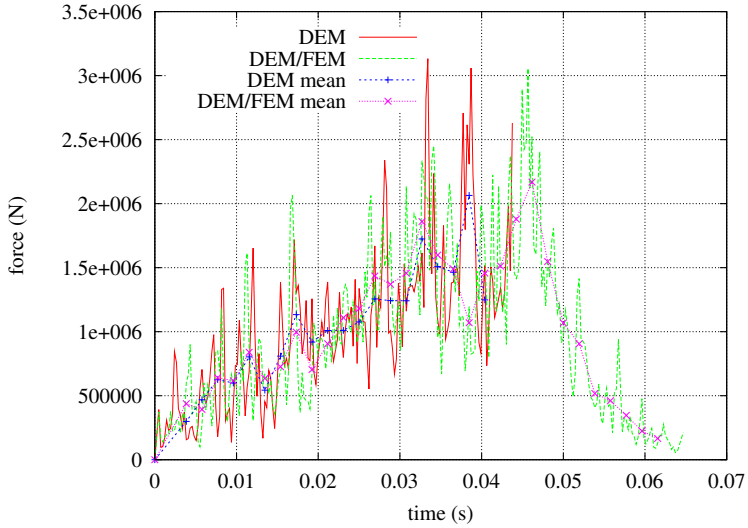

Figure 18: Cutting force histories for DEM and hybrid DEM/FEM simulations of rock cutting

3 NUMERICAL PREDICTION OF WEAR OF ROADHEADER PICKS

3.1 Introduction

Wear of cutting tools is one of the decisive factors in progress of excavation works [18]. Changes of bit geometry due to wear lead to difficulties in cutterhead penetration reducing thus cutting performance. High tool wear can be one of the main problems in roadheader excavation.

Practical observations show that different wear mechanisms can occur in roadheader picks [1]. Figure 19 shows typical examples of worn roadheader picks. Abrasive wear (Fig. 19a) is one of

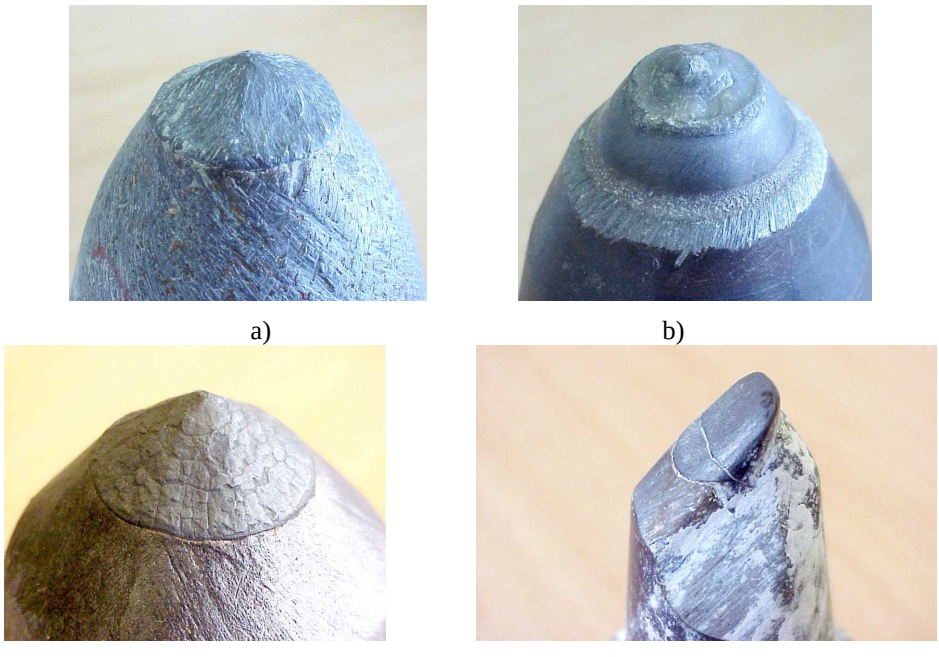

Figure 19: Different pick failure mechanisms in cutting of hard rocks: a) abrasive wear, b) adhesive wear, c) surface fatigue and abrasion, d) adhesion and fatigue (from [1])

the most important mechanisms in cutting of hard rocks especially in the presence of quartzite.

Scraping of the rock surface leads to high temperatures, which softens the steel body and hard-metal tip, resulting in increasing wear of adhesive character (Fig. 19b). Adhesive wear is typical for heat generating rock of low abrasivity (Fig. 19d). In the field of rock and ground excavation it is very rare that just one wear mechanism occurs. Different mechanisms can act in parallel, as it is shown for instance Figs. 19c,d.

Wear of rock cutting tools depends on many factors, the following ones have been identified as the most important [19]: rock/soil properties (strength, hardness, fracture properties, brittleness, abrasive capacity), tool characteristics (material properties, strength, hardness, geometry), cutting process parameters (position of a tool with respect to rock (penetration depth, rake and cutting angles, cutting velocity, cutting forces, heat generation, cooling, temperature).

A critical issue in successful roadheader application is the ability to predict reliable estimates of machine production capacity (ICR) and the associated bit consumption rate (BCR). Based on the past experience and the statistical interpretation of the previous case histories different empirical performance prediction methods have been developed, cf. [18, 3]. Bit consumption rate is correlated with the wear. The main motivation of the research work presented in this paper is development of the numerical model increasing possibilities to predict abrasive and adhesive wear of roadheader picks (bits) under different process conditions. This will allow an optimum design of excavation process maximizing the cutting rate and minimizing the bit consumption rate. In the approach adopted the wear is evaluated based on the simulation of rock cutting process.

3.2 Numerical model of rock cutting

3.2.1 *Basic assumptions*

A numerical model of the tool-rock system allowing us to simulate a process of rock cutting has been developed within the framework of the discrete element method (DEM) [16]. In this model a rock material is represented as a collection of rigid spherical (in 3D) or cylindrical (in 2D) particles interacting among themselves with contact forces. Discrete element formulation using spherical or cylindrical particles was first proposed by Cundall and Strack [5, 4]. The present model has been developed within the implementation of DEM described in [17, 12].

In the model of rock cutting, the tool is considered rigid, assuming that its stiffness is sufficient to produce rock failure and its deformation is irrelevant for the purposes of modelling of rock failure. The tool-rock interaction is modelled assuming Coulomb friction model

3.2.2 *Discrete element method formulation*

The translational and rotational motion of rigid spherical or cylindrical elements (particles) is governed by the standard equations of rigid body dynamics. For the i-th element we have

$$m_i \ddot{\mathbf{u}}_i = \mathbf{F}_i \,, \tag{57}$$

$$I_i \dot{\boldsymbol{\omega}}_i = \mathbf{T}_i \,, \tag{58}$$

where $\mathbf{u}$ is the element centroid displacement in a fixed (inertial) coordinate frame $\mathbf{X}$, $\boldsymbol{\omega}$ – the angular velocity, m – the element mass, I – the moment of inertia, $\mathbf{F}$ – the resultant force, and $\mathbf{T}$ – the resultant moment about the central axes. Equations of motion (57) and (58) are integrated in time using the central difference scheme [16].

Vectors $\mathbf{F}$ and $\mathbf{T}$ are sums of all forces and moments applied to the i-th element due to external load, contact interactions with neighbouring spheres and other obstacles, as well as

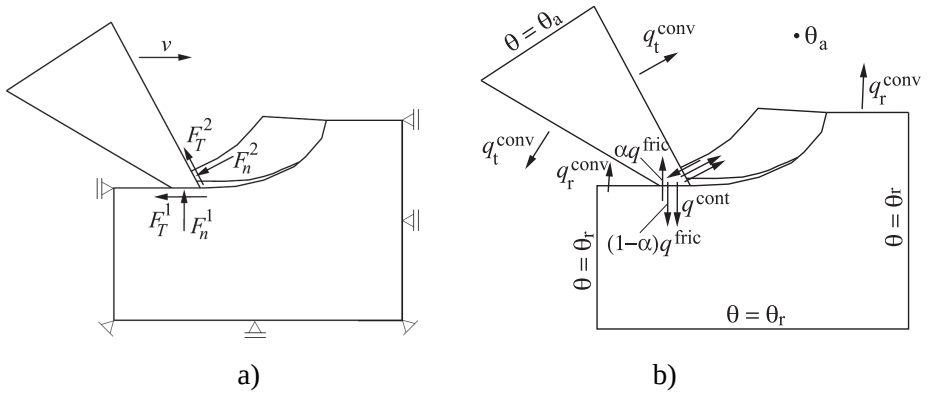

Figure 20: Thermo-mechanical model of rock cutting: a) scheme of mechanical problem, b) scheme of thermal problem.

forces resulting from damping in the system. The contact force between two elements $\mathbf{F}$ can be decomposed into normal and tangential components, $\mathbf{F}_n$ and $\mathbf{F}_T$, respectively

$$\mathbf{F} = \mathbf{F}_n + \mathbf{F}_T = F_n \mathbf{n} + \mathbf{F}_T \,, \tag{59}$$

where $\mathbf{n}$ is the unit vector normal to the particle surface at the contact point.

The contact forces F_n and $\mathbf{F}_T$ are obtained using a constitutive model formulated for the contact interaction. Rock materials are modelled using elastic perfectly brittle model [16], where we assume initial bonding for the neighbouring particles. These bonds can be broken under load allowing us to simulate initiation and propagation of material fracture. After debonding the elements can interact assuming standard frictional contact conditions without cohesion. Similarly the fricitional contact is assumed for the tool-rock interaction. In the present formulation the Coulomb model is adopted for friction.

3.2.3 *Thermomechanical model of rock cutting*

Thermal effects are important factors influencing the tool wear in rock cutting. High temperatures developed on the surface (in some cases temperature on the tool surface can reach as much as 550–800°C, cf. [19, 9] due to heat generated by friction between tool and rock reduce the hardness of the surface and increase adhesive and abrasive wear.

Evaluation of wear requires determination of forces of cutting as well as temperature distribution. This means necessity to analyse rock cutting as a thermo-mechanical process. Temperature increases due to heat generated by friction between tool and rock. Heat is adsorbed and conducted by the tool and rock. Thermo-mechanical model of rock cutting shown schematically in Fig. 20 has been developed in [14].

Thermal phenomena during rock cutting are described by the heat balance equation. This equation can be written for a single particle in the following form:

$$m_i c \dot{T}_i = Q_i \,, \tag{60}$$

where: m_i – particle mass, c – specific heat, T_i – particle temperature, Q_i – heat sources or heat fluxes per single particle. Q_i includes externally supplied heat source Q_i^{ext}, heat generated through friction dissipation and absorbed by the particle Q_{ij}^{gen}, heat conducted through the

contact interface $Q_{ij}^{\rm cont}$, and convective and radiative heat transfer between particles and environment on the free surface, $Q_i^{\rm conv}$ and $Q_i^{\rm rad}$

$$Q_i = Q_i^{\rm ext} + \sum_{j=1}^{n_c} Q_{ij}^{\rm gen} + \sum_{j=1}^{n_c} Q_{ij}^{\rm cont} + Q_i^{\rm conv} + Q_i^{\rm rad} \tag{61}$$

where n_c is the number of particles being in contact with the i-th particle.

Particle-to-particle conductive heat transfer rate $Q_{ij}^{\rm cont}$ is assumed in the form analogical to the Fourier equation

$$Q_{ij}^{\rm cont} = h^{\rm cond}(T_i - T_j) \tag{62}$$

with $h^{\rm cond}$ being the heat transfer coefficient between material particles, which can be determined as a function of the solid heat conductivity and particle configuration.

Heat generation through frictional dissipation is calculated using the following formula

$$Q_i^{gen} = \chi \left| F_T \, v_T \right| , \tag{63}$$

where F_T is the friction force, v_T is the relative tangential velocity, and $0 \leq \chi \leq 1$ is the part of the friction work converted to heat.

Thermo-mechanical coupled problem defined by Eqs. (57), (58) and (60) is solved using the staggered solution scheme, in which the mechanical and thermal problems are analysed separately. The two problems are coupled by heat generation process – heat generated by friction is evaluated in the solution of mechanical problem and passed to the solution of thermal problem.

3.3 Wear model

3.3.1 *Archard model of wear*

Among the quantitative models of wear the classical formula of Archard [2] is still widely used. It assumes that the wear rate $\dot{w}$ is proportional to the contact pressure p_n and to the slip velocity v_T

$$\dot{w} = k \frac{p_n v_T}{H} , \tag{64}$$

where H denotes the hardness of worn surface and k is a dimensionless wear parameter. The Archard model was derived originally for adhesive wear, the same form of equation, however, can be obtained for abrasive wear, cf. [13]. Values of adhesive and abrasive wear constants k for different combinations of materials can be determined in laboratory tests. It is commonly accepted that wear is related to friction and thus friction coefficients are often introduced into Eq. (64). If Coulomb friction holds

$$p_T = \mu p_n \tag{65}$$

μ being the friction coefficient, the Archard wear law can be written in the following equivalent form:

$$\dot{w} = \bar{k} \frac{p_T v_T}{H} = \bar{k} \frac{\dot{D}}{H} \tag{66}$$

3.3.2 *Wear model accounting for thermal effects*

Influence of temperature on wear can be taken into account by adaptation of the law of Archard [2] given by Eq. (64). Thermal effects can be captured approximately by taking hardness H changing with temperature T

$$H = H(T) \tag{67}$$

Taking this into account in Eq. (64) we have

$$\dot{w} = k\frac{p_n v_T}{H(T)} \tag{68}$$

Analogically Eq. (66) takes the form:

$$\dot{w} = \bar{k}\frac{p_T v_T}{H(T)} = \bar{k}\frac{\dot{D}}{H(T)} \tag{69}$$

3.3.3 *Numerical implementation of wear evaluation algorithm*

The tool wear w, i.e. the amount (depth) of removed material is obtained by integrating the wear rate $\dot{w}$ in time

$$w = \int \dot{w}\,\mathrm{d}t\,. \tag{70}$$

The Archard law given by Eq. (69) has been implemented in the numerical algorithm. Distribution of wear on the tool surface can be estimated and the tool shape can be modified according to the calculated wear.

Wear is a relatively slow process and it can be observed after many work cycles. In the numerical algorithm developed wear is accelerated using scaled wear constants. Thus visible wear is obtained in one cycle analysed.

The developed numerical algorithm of wear evaluation takes advantage of the tool discretization with distinct elements. This will allow us to easily modify the shape of the tool. The tool shape is changed eliminating particles if the accumulated wear exceeds the particle diameter. The tool shape is modified continuously during the analysis.

3.4 Simulation of rock cutting with wear evaluation

Simulation of rock cutting with one pick of a roadheader has been analysed using a model shown in Fig. 21. A sample of rock and one pick of a cutter head have been modelled. Mechanical properties of the rock are assumed the same as for the sandstone studied experi-

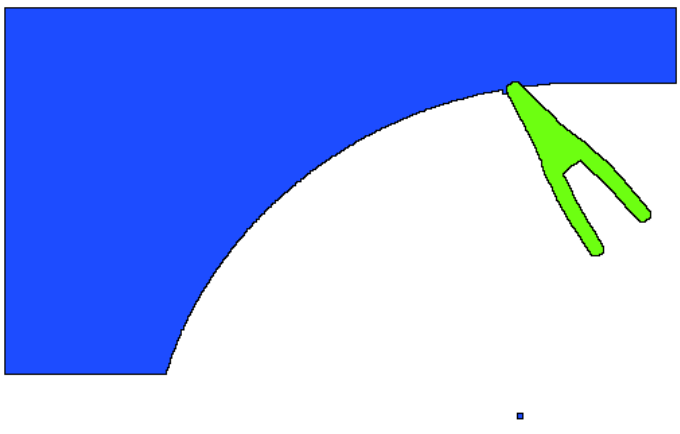

Figure 21: Model geometry for simulation of rock cutting with one pick of a roadheader

mentally and numerically in [16]: Young modulus $E = 18690$ MPa, Poisson ratio $\nu = 0.23$, unconfined compression strength $\sigma_c = 127.8$ MPa, and tensile strength $\sigma_t = 12.3$ MPa.

Material sample is represented by an assembly of randomly compacted 92000 discs of radii 1–1.5 mm. Model parameters obtained for sandstone in [16] are assumed for the micromechanical model. For the rock–tool interaction the following set of parameters has been assumed: $k_{\mathrm{n}} = k_{\mathrm{s}} = 5 \cdot 10^{10}$ MPa, $\mu = 0.4$.

The swing velocity of the cutter head was assumed 0.2 m/s, and angular velocity 1.6204 s^{-1}, which with the distance of the tooth from the axis of rotation 0.7 m gives circumferential velocity 1.134 m/s.

Thermomechanical analysis with wear evaluation has been carried out. Results of the analysis are shown in Figs. 22–24. Failure of rock during cutting is shown in Fig. 22. Failure typical for brittle rock can be observed. Temperature evolution is shown in Fig. 23, the highest temperature is observed in the contact zones, where the frictional heat is generated. The same area has maximum wear amounts as it is shown in Fig. 24

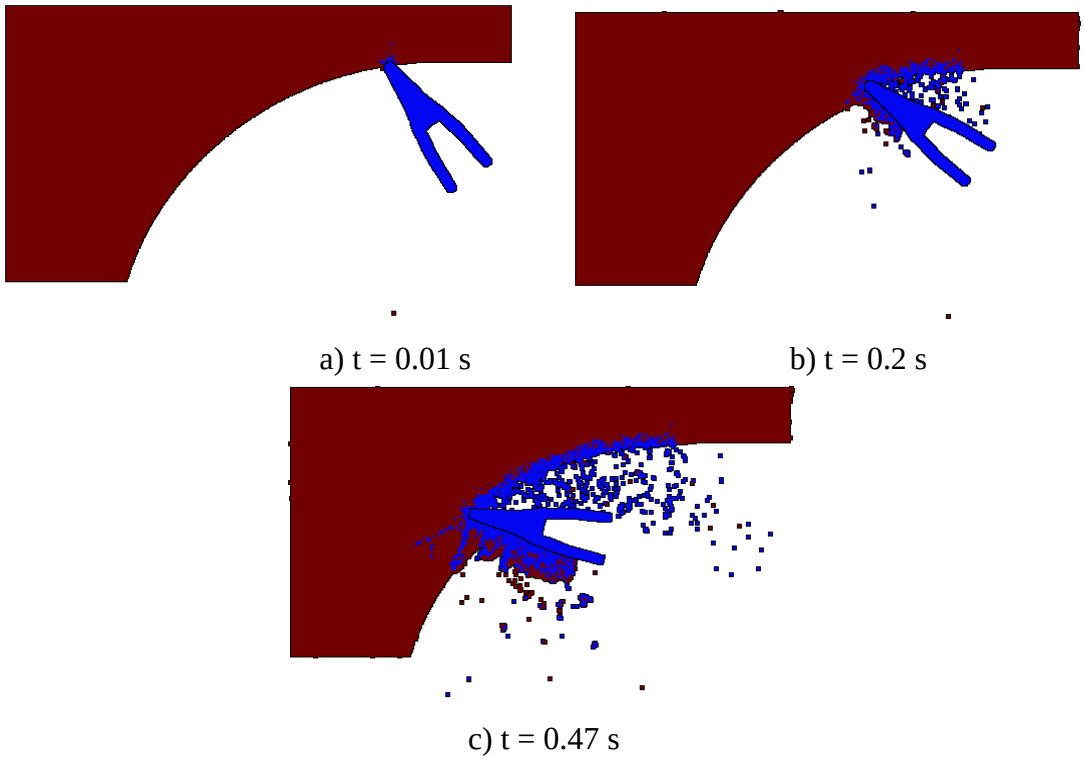

Figure 22: Simulation of rock cutting by a pick of a road header – failure mode for the discrete element model

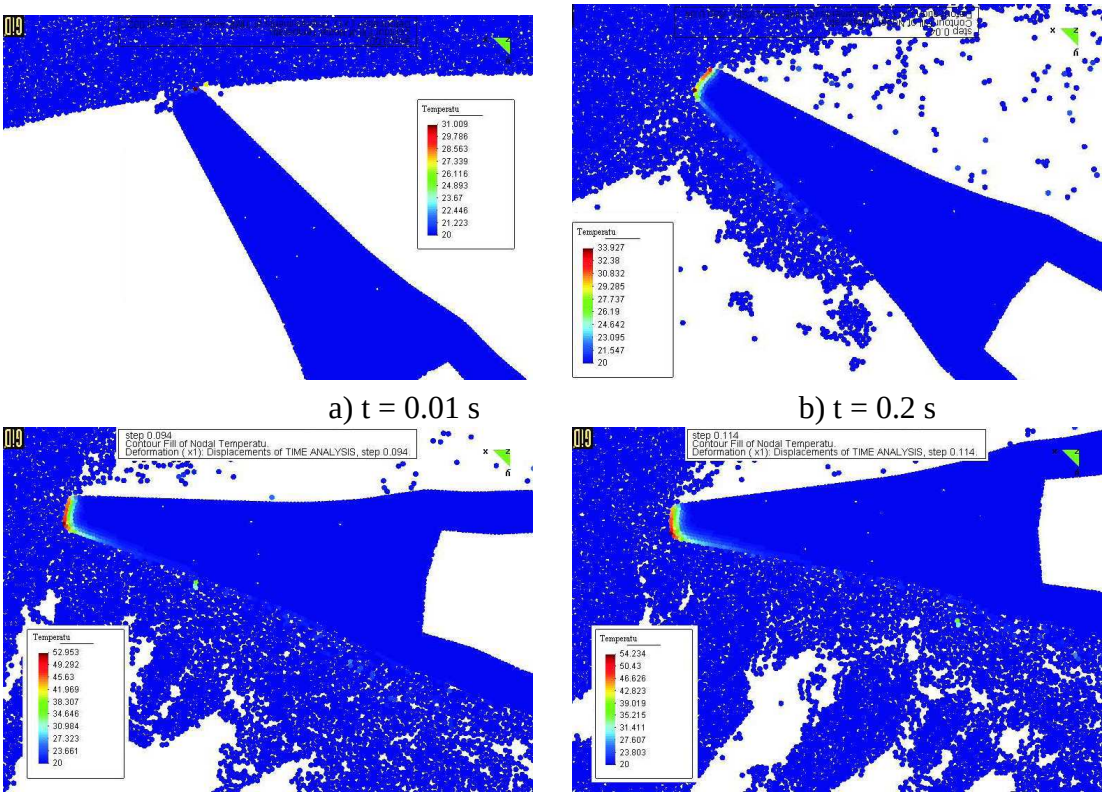

a) t = 0.01 s b) t = 0.2 s

c) t = 0.47 s d) t = 0.57 s

Figure 23: Simulation of rock cutting with one pick of a road header – temperature evolution

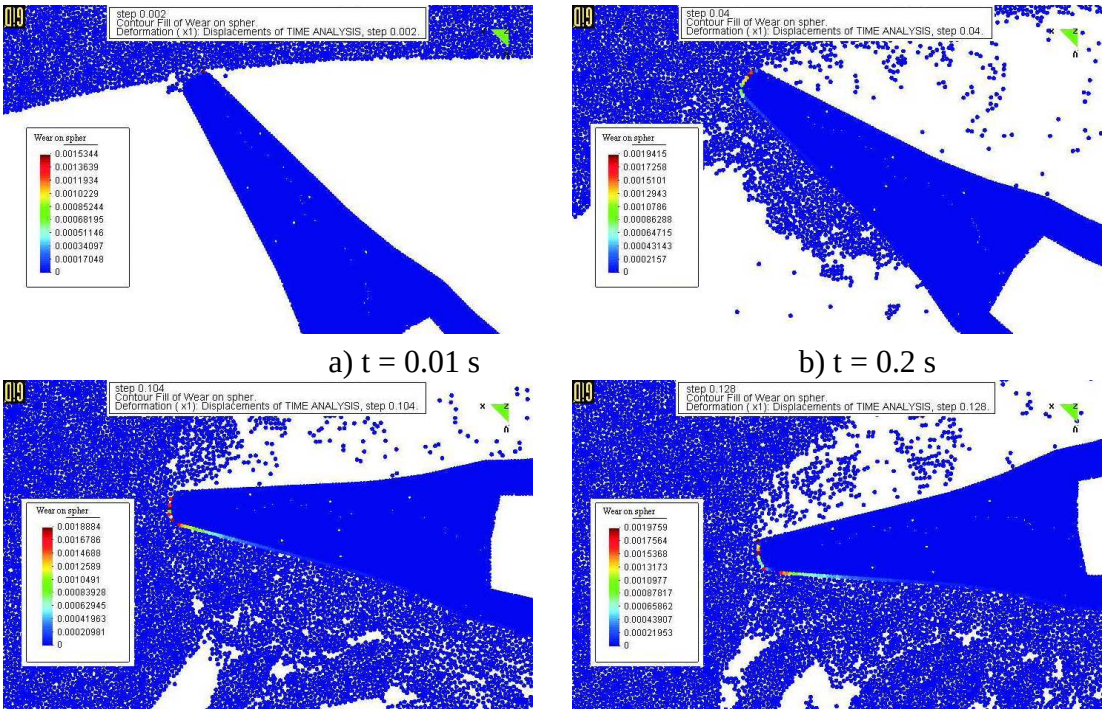

a) t = 0.01 s b) t = 0.2 s

c) t = 0.47 s d) t = 0.57 s

Figure 24: Simulation of rock cutting with one pick of a road header – accumulated wear on the tool surface

4 CONCLUSIONS

- Numerical simulation using the discrete element method predicts correctly the failure mode in cutting of brittle rocks with roadheader picks.
- Numerical analysis provides estimation of cutting forces. Numerical results of 2D simulation show reasonable agreement with experimental data.
- The methodology developed can be useful in the quantification of influences of different parameters on the cutting process and finally in the design of cutting units.
- The combination of discrete and finite elements is an effective approach for simulation of undeground rock excavation.
- Advantages of combined modelling:
  - taking advantage of strong sides of each method, avoiding disadvantages,
  - better representation of physical phenomena,
  - improving numerical efficiency.
- DEM/FEM coupling has been implemented using different methods (Lagrange multipliers, penalty, overlapping and non-overlapping DEM and FEM subdomains)
- Evaluation of wear has been introduced into the tool-rock interaction model.
- Extension of the discrete element formulation on thermal and thermomechanical problems allows us to take into account thermal effects in the wear evaluation.
- The methodology developed enables estimation of wear amount as well as prediction of shape evolution due to wear
- In future work influence of different operating parameters and conditions on wear will be studied.
- Further studies will include laboratory tests to determine wear parameters, required wear constants can be estimated using the Cerchar scratch test and linear rock cutting experiments.

REFERENCES

[1] J. Akerman. *Wear of rock cutting tools*. VOEST-ALPINE Bergtechnik, 2006.

[2] J.F. Archard. Contact and rubbing of flat surfaces. *J. Appl. Phys.*, 24(8):981–988, 1953.

[3] H. Copur, L. Ozdemir, J. Rostami, and N. Bilgin. Studies on performance prediction of roadheaders based on field data in mining and tunneling projects. In *Int. 4th Mine Mechanization and Automation Symp.* Brisbane, Australia, 1997.

[4] P.A. Cundall. Formulation of a Three Dimensional Distinct Element Model — Part I. A Scheme to Detect and Represent Contacts in a System of Many Polyhedral Blocks. *Int. J. Rock Mech., Min. Sci. & Geomech. Abstr.*, 25(3):107–116, 1988.

[5] P.A. Cundall and O.D.L. Strack. A discrete numerical method for granular assemblies. *Geotechnique*, 29:47–65, 1979.

[6] I. Evans. The force required for pointed attack picks. *Int. J. Min. Engng.*, 2:63–71, 1965.

[7] H. Huang. *Discrete Element Modeling of Tool-Rock Interaction*. PhD thesis, University of Minnesota, 1999.

[8] J. Jonak and J. Podgórski. Mathematical model and results of rock cutting modelling. *Journal of Mining Science*, 37:615–618, 2001.

[9] J.P. Loui and U.M. Rao Karanam. Heat transfer simulation in dragpick cutting of rocks. *Tunnelling and Underground Space Technology*, 20:263–270, 2005.

[10] D.M. Neil, J. Rostami, L. Ozdemir, and R.E. Gertsch. Production estimating techniques for undeground mining using roadheaders. In *Annual meeting of the Society of Mining Metallurgy and Exploration Engineers*. Albuquerque, 1994.

[11] Y. Nishimatsu. The mechanics of rock cutting. *Int. J. Rock Mech. Mining Sci.*, 9:261–270, 1972.

[12] E. Oñate and J. Rojek. Combination of discrete element and finite element methods for dynamic analysis of geomechanics problems. *Comput. Meth. Appl. Mech. Eng.*, 193:3087–3128, 2004.

[13] E. Rabinowicz. *Friction and wear of materials*. John Wiley & Sons, 1995.

[14] J. Rojek. *Modelling and simulation of complex problems of nonlinear mechanics using the finite and discrete element methods* (in Polish). Habilitiation Thesis, Institute of Fundamental Technological Research Polish Academy of Sciences, Warsaw, 2007.

[15] J. Rojek, Jan Akerman, E. Oñate, and F. Zarate. Numerical prediction of wear of roadheader picks. In *ECCOMAS Thematic Conference on Computational Methods in Tunnelling EURO:TUN-2007*, Vienna, Austria, August 27-29, 2007.

[16] J. Rojek, H. Kargl, U. Restner, and E. Oñate. Simulation of rock cutting in undeground excavation with roadheaders. In *ECCOMAS Thematic Conference on Computational Methods in Tunnelling EURO:TUN-2007*, Vienna, Austria, August 27-29, 2007.

[17] J. Rojek, E. Oñate, F. Zarate, and J. Miquel. Modelling of rock, soil and granular materials using spherical elements. In *2nd European Conference on Computational Mechanics ECCM-2001*, Cracow, 26-29 June, 2001.

[18] K. Thuro and R.J. Plinninger. Predicting roadheader advance rates. *Tunnels & Tunneling International*, (6):36–39, 1999.

[19] P.N.W. Verhoef. *Wear of rock cutting tools*. Balkema, Rotterdamd, 1997.

[20] S.P. Xiao and T. Belytschko. A bridging domain method for coupling continua with molecular dynamics. *Comput. Meth. Appl. Mech. Eng.*, 193:1645–1669, 2004.

[21] Y. Yua, J. Yinb, and Z. Zhong. Shape effects in the Brazilian tensile strength test and a 3D FEM correction. *Int. J. Rock Mech. Min. Sci.*, 43:623–627, 2006.